ResearchGate

See discussions, stats, and author profiles for this publication at: https://www.researchgate.net/publication/44158376

Assessing future nitrogen deposition and carbon cycle feedback using a multimodel approach: Analysis of nitrogen deposition

Article *in* Journal of Geophysical Research Atmospheres · October 2005

DOI: 10.1029/2005JD005825 · Source: OAI

CITATIONS
301

READS
296

20 authors, including:

Jean-François Lamarque
National Center for Atmospheric Research
488 PUBLICATIONS **65,200** CITATIONS

SEE PROFILE

Jeffrey T. Kiehl
University of California, Santa Cruz
235 PUBLICATIONS **34,044** CITATIONS

SEE PROFILE

Guy P. Brasseur
Max Planck Institute for Meteorology
419 PUBLICATIONS **23,251** CITATIONS

SEE PROFILE

Tim Butler
IASS Institute for Advanced Sustainability Studies Potsdam
133 PUBLICATIONS **8,125** CITATIONS

SEE PROFILE

Some of the authors of this publication are also working on these related projects:

Thesis View project

Regional Air Pollution View project

All content following this page was uploaded by Larry W Horowitz on 19 May 2014.

The user has requested enhancement of the downloaded file.

Assessing future nitrogen deposition and carbon cycle feedback using a multi-model approach. Part 1: Analysis of nitrogen deposition.

J.-F. Lamarque[1], J. Kiehl[1], G. Brasseur[2], T. Butler[3], P. Cameron-Smith[4], W. D. Collins[1], W. J. Collins[5], C. Granier[2,6,7], D. Hauglustaine[8], P. Hess[1], E. Holland[1], L. Horowitz[9], M. Lawrence[3], D. McKenna[1], P. Merilees[1], M. Prather[10], P. Rasch[1], D. Rotman[4], D. Shindell[11] and P. Thornton[1]

[1]National Center for Atmospheric Research, Boulder, CO, U.S.A

[2]Max-Planck Institute for Meteorology, Hamburg, Germany

[3]Max-Planck Institute for Chemistry, Mainz, Germany

[4]Lawrence Livermore National Laboratory, Livermore, CA, U.S.A.

[5]Hadley Centre, Met Office, Exeter, U.K.

[6]Service d'Aéronomie/Institut Pierre-Simon Laplace, Paris, France

[7]CIRES/NOAA Aeronomy Laboratory, Boulder, CO, U.S.A.

[8]Laboratoire des Sciences du Climat et de l'Environnement/Institut Pierre-Simon Laplace, Paris, France

[9]National Oceanic and Atmospheric Administration, Princeton, N.J., U.S.A.

[10]University of California, Irvine, CA, U.S.A

[11]NASA Goddard Institute for Space Studies, New York, NY, U.S.A.

Abstract. In this study, we present the results of nitrogen deposition from a set of 28 simulations from 6 different tropospheric chemistry models pertaining to present-day and 2100 conditions. We show that, under the assumed A2 scenario, the global annual average nitrogen deposition over land is expected to increase three-fold, mostly due to the increase in nitrogen emissions. This will create large areas where the annual average nitrogen deposition rate exceeds 1 gN/m^2. Using the results from all models, we have documented the strong linear relationship between models on the fraction of the nitrogen emissions that is deposited, regardless of the emissions (present-day or 2100). On average, approximately 70% of the emitted nitrogen is deposited over land. For present-day conditions, the results form this study suggest that the deposition over land ranges between 25 and 40 Tg(N)/year. By 2100, under the A2 scenario, the deposition over land is expected to range between 60 and 80 Tg(N)/year. Over forests, the deposition is expected to increase from 10 Tg(N)/year to 20 Tg(N)/year. Nitrogen deposition changes from changes in the climate change accounts for less than the modeled total changes in 2100.

1. Introduction

The terrestrial biosphere plays a critical role in the global carbon cycle [*Schimel*, 1995]. While a variety of factors affects the carbon cycle in the terrestrial biosphere (temperature, precipitations, CO_2 concentration, land-use changes, etc.), it has recently become evident that nitrogen deposition is a key constraint on the net primary productivity [*Vitousek et al*., 1997; *Prentice et al*., 2001]. Increases in fossil-fuel use and

a growing population during the 20th century have led to a large increase in nitrogen deposition [*Holland et al*., 1997, 2004; *Vitousek et al*., 1997]. However the impact of this perturbation to the nitrogen cycle on the global carbon cycle is uncertain as inconsistencies in the ecosystem response exist between models and observations [*Holland et al*., 1997; *Jenkinson et al*., 1999; *Nadelhoffer et al*., 1999; *Throop et al*., 2004]. In particular, it is likely that some ecosystems have been positively affected by this added fertilization and may have increased their carbon sequestration [*Sievering*, 1999]. Possibly, this increased carbon sequestration could explain a significant fraction of the CO_2 "missing sink" [*Schimel*, 1995; *Townsend et al*., 1996; *Holland et al*., 1997], although this assessment is being disputed [*Nadelhoffer et al*., 1999; *Prentice et al*., 2001]. On the other hand, for heavily deposited regions, sustained C sinks are unlikely [*Schulze et al*., 1989]. In addition, nitrogen-enhanced CO_2 uptake may eventually become limited by soil acidification and ozone pollution, as these effects are usually present in combination with large nitrogen deposition rates [*Ollinger et al*., 2002; *Holland et al.,* 2005]. The potential feedback between nitrogen deposition and carbon uptake could become a critical component to the evolution of the climate and needs to be assessed. As a first analysis, only the nitrogen deposition impact on vegetation is being considered in this study. In the next phase of this study, we will calculate if the potential increased plant productivity from increased nitrogen fertilization will be able to absorb significant amounts of carbon dioxide.

During the 21st century, nitrogen emissions from anthropogenic sources are expected to further increase dramatically; in particular, in the A2 IPCC SRES scenario[*Prather et al*., 2001], the tropical regions are expected to at least double or triple

their present-day emissions. Nitrogen emissions are in the form of nitrogen oxide (NO) or dioxide (NO_2). Following their emissions, the released nitrogen undergoes a series of chemical transformations (oxidation or heterogeneous reactions on particles) and deposition; this deposition can be in the form of dry deposition at the surface or wet removal in the presence of rain (mostly in the form of HNO_3). It is clear that deposition of nitrogen on land will increase in response to the increase in emissions. But it is unclear how large this increase will be and how dependent it will be on the climate system.

To tackle the problem of the impact of nitrogen deposition, we have devised a multi-model approach with the goal of providing a lower bound on the nitrogen deposition uncertainty; parameters not considered in this study can only increase the range of estimates. For that purpose, we use a variety of models to create an ensemble from which statistics can be deduced. These models are a blend of climate models with interactive chemistry and chemistry-transport models. To increase the spread of the ensemble members, while we have decided to focus on only the IPCC SRES A2 [*Prather et a*l., 2001] scenario (which, being the worst case scenario, will provide an upper limit on the nitrogen emissions and therefore deposition), the chemical surface emissions were left unconstrained, even for present-day conditions. Finally, to reduce the computational burden, only simulations for 2000 and 2100 were performed.

In this first part, we will analyze the nitrogen deposition fields and provide sensitivities to climate and emissions. The second part of this analysis will focus on the impact on the carbon cycle, using the deposition fields described in this paper as forcings to a land model, and will be described in a future paper. This full modeling exercise was

named by the members of this group as the SANTA FE project (Scientific Analysis of Nitrogen cycle Towards Atmospheric Forcing Estimation).

The paper is organized as follows: in section 2, we briefly describe the models involved in the simulations, both climate and chemistry. We discuss the design of the simulations in section 3 while the boundary conditions (sea-surface temperatures and emissions) are discussed in section 4. The analysis of the modeled nitrogen deposition fields is done in section 5, including a comparison with deposition climatologies. Conclusions are drawn in section 6.

2. Models

For this study, a total of twenty-eight simulations from 6 groups were performed (see Table 1) in order to examine the sensitivity of the nitrogen deposition to a variety of factors. These include sensitivity to climate (forced by changes in sea-surface temperatures (SSTs)) and to emissions, including sensitivity to the lightning source of NO. Only the simulations for present-day conditions and combined 2100 climate and 2100 emissions were mandatory for this study.

In order to create a variety of climate conditions for present and future conditions, we have first created four sets of monthly-averaged sea-surface temperatures (Figure 1; also see discussion in section 4) using a 10-year climatology based on results from coupled models from the following institutions: GISS, HadCM, IPSL and NCAR (see below for a definition of these acronyms). The 2100 conditions were provided by each group as perturbations from the present-day. This perturbation field was then added to each participating climate model SST field to provide a range of climate forcings. The use of perturbation fields limits the propagation of biases across models.

Using the set of four different SST fields available, four atmospheric general circulation models (GCMs) simulated the present-day and 2100 climates. In addition, three models (GISS, HadCM and IPSL) performed the chemical simulations interactively using a variety of SST forcings; NCAR created the meteorological fields necessary for the off-line chemistry-transport models.

To limit the space dedicated to model description in this paper, we are only highlighting the main features of interest regarding this study. The reader is referred to other publications for more details. A brief section summarizing the specifics most relevant to nitrogen deposition is given in section 2.3.

2.1. General circulation models

2.1.1. NASA Goddard Institute for Space Science (GISS)

The tropospheric chemical scheme in the new GISS model III/modelE general circulation model [*Schmidt et al.*, 2004] is the same as that used in the earlier model II', and includes basic HO_x-NO_x-O_x-CO-CH_4 chemistry and lumped families of peroxy-acetyl nitrates (PANs) and higher non-methane hydrocarbons (isoprene, alkyl nitrates, aldehydes, alkenes, and paraffins) [*Shindell et al.*, 2003]. It uses 77 reactions among 32 species, 16 of which are transported within the GCM. Calculations are performed using a chemical time step of 1/2 hour. The chemistry is fully coupled with a model sulfate aerosol model, which includes DMS, MSA, SO_2 and sulfate. Hence heterogeneous hydrolysis of N_2O_5 into HNO_3 takes place on variable sulfate areas while sulfate oxidation depends upon gas-phase chemistry. Photolysis rates are calculated every hour and interact with the model aerosol and cloud fields. Phase transformations of soluble

species are calculated based on the GCM internal cloud scheme. We include transport within convective plumes, scavenging within and below updrafts, rainout within both convective and large-scale clouds, washout below precipitating regions, evaporation of falling precipitation, and both detrainment and evaporation from convective plumes. ModelE includes a cloud tracer budget for the trace gas and aerosol species rather than returning dissolved material to the gas-phase at the end of each timestep. The model also includes a new dry deposition module, based on a resistance-in-series calculation and prescribed (i.e. uncoupled) vegetation, which is physically consistent with the other surface fluxes (e.g. water, heat) in the planetary boundary layer scheme. Chemical calculations are performed up to the tropopause. Lightning NO_x is based on the *Price et al.* [1997] scheme. A set of simulations was performed using a development version of modelE (hereafter identified by GISS1), which were then repeated using the release version of the GCM (GISS2).

The model reproduction of observed aspects of ozone and related trace gases is improved over our earlier studies [*Shindell et al.*, 2003]. The overestimate of ozone in the vicinity of 300 mb has been reduced by half (to 13%), and biases are now less than 10% at all other levels based on the month-by-month differences between the model and 16 recommended ozonesonde sites [*Logan*, 1999]. The ozone bias near the surface (900 hPa) is –1.4 ppbv (5%). The model overpredicts HNO_3 and PAN in polluted regions (including biomass burning regions) by a factor of two to four, somewhat less than previously [*Shindell et al.*, 2003] owing to the liquid tracer budget. Recent simulations including reactions on dust greatly ameliorate these biases in the Northern Hemisphere, and only marginally alter NO_x which agrees with observations quite well in both polluted and

remote areas. Precipitation in modelE is generally well-simulated over North America, though it is slightly underpredicted over Europe [*Schmidt et al.*, 2004]. The configuration here is a 23-layer version with a top at 0.015 hPa and a $4^{o}x5^{o}$ horizontal resolution.

2.1.2. Hadley Centre (HadCM)

STOCHEM is a parcel trajectory model, which is run coupled to the Met Office HadCM3 climate model. The climate model has 19 levels up to a model top of 4.6 hPa, and a timestep of 30 min. Time steps for advection and chemistry are 60 and 5 min, respectively. STOCHEM subdivides the model domain in 50,000 parcels. The model uses a chemistry scheme involving oxidation of hydrocarbons up to C4 and isoprene. Downward ozone fluxes (500 Tg/year) are prescribed across the 100 hPa surface. Isoprene emissions are parameterized according to *Guenther et al.* [1995]. Lightning NO_x emissions are parameterized according to *Price and Rind* [1994]. Methane emissions from wetland are interactively calculated as described in *Gedney et al*. [2004]. Dry deposition is interactively coupled to the land surface, depending on soil moisture, leaf area index and stomatal conductance. Wet deposition is parameterized according to *Penner et al.* [1994]. For a complete model description see *Sanderson et al.* [2003].

2.1.3. Institut Pierre-Simon Laplace (IPSL)

The LMDz (Laboratoire de Météorologie Dynamique, zoom) model is a grid point General Circulation Model (GCM) developed initially for climate studies by *Sadourny and Laval*, [1984]. In LMDz the finite volume transport scheme of *Van Leer*, [1977] is used to calculate large-scale advection of tracers. The parameterization of deep convection is based on the scheme of *Tiedke*, [1989]; a local second-order closure

formalism is used to describe turbulent mixing in the planetary boundary layer (PBL). LMDz (version 3.3) has a horizontal resolution of 3.8 degrees in longitude and 2.5 degrees in latitude and uses 19 vertical σ-p levels extending from the surface to 3 hPa.

The Interactive Chemistry and Aerosols (INCA) model has been integrated into LMDz. INCA includes 85 chemical species and 303 chemical reactions, and simulates tropospheric chemistry, emissions, and deposition of primary tropospheric trace species including non-methane hydrocarbons. The anthropogenic emission inventory is based on EDGAR V3.0 [*Olivier et al.*, 2001]. Biomass burning emissions are introduced in the model according to the satellite based inventory developed by *Van der Werf et al.*, [2003]. The ORCHIDEE (Organizing Carbon and Hydrology in Dynamic Ecosystems) dynamical vegetation model [*Krinner et al.*, 2004] has been used to provide biogenic surface fluxes of isoprene, terpenes, acetone, and methanol. A detailed description and evaluation of LMDz-INCA can be found in *Hauglustaine et al.*, [2004] and *Folberth et al.*, [2004].

2.1.4. National Center for Atmospheric Research (NCAR)

Two separate models were used by the NCAR group: first, the Community Atmospheric Model (CAM) was used to create the meteorological datasets needed to run the chemistry/transport models. Then the NCAR chemistry/transport model MOZART-2 (Model for Ozone And Related chemical Tracers, version 2) was run to simulate the 2000 and 2100 chemical states. This latter model is described below with the other off-line chemistry transport models.

The Community Atmosphere Model (CAM3) represents the sixth generation of atmospheric general circulation models (AGCMs) developed by the climate community

in collaboration with the National Center for Atmospheric Research (NCAR). CAM3 can be run either as a stand-alone AGCM or as a component of the Community Climate System Model (CCSM) [*Collins et al*., 2004a]. In its stand-alone mode, CAM3 is integrated together with the Community Land Model [*Bonan et al*. 2002; *Oleson et al. 2004*], a thermodynamic sea ice model, and an optional slab-ocean model [*Hack et al*. 2004]. For more details, see *Collins et al*. [2004b]

The treatments of microphysics and cloud condensate have been substantially revised in CAM3 [*Boville et al*., 2004]. The cloud-water is predicted from the prognostic cloud-water parameterization of *Rasch and Kristjánsson* [1998] updated by *Zhang et al*. [2003]. The new model includes separate evolution equations for the liquid and ice-phase condensate. The revised scheme includes a new formulation of the fractional condensation rate and a self-consistent treatment of the evolution of water vapor, heat, cloud fraction, and in-cloud condensate [*Zhang et al*. 2003].

In its default configuration, CAM3 includes the radiative effects of an aerosol climatology in its calculation of shortwave fluxes and heating rates. The new aerosol data set includes the annually-cyclic, monthly-mean distributions of sulfate, sea-salt, carbonaceous, and soil-dust aerosols. The climatology is derived from a chemical transport model constrained by assimilation of satellite retrievals of aerosol depth [*Collins et al*. 2001; *Rasch et al*. 2001]. The climatology in CAM3 is obtained from an aerosol assimilation for the period 1995–2000. For this work, CAM3 was run at a horizontal resolution of T42 and the nominal vertical resolution of 26 levels.

2.2. Off-line chemistry-transport models

In all cases, the off-line chemistry models listed below used the meteorological fields created by the NCAR GCM (see section 2.1.4) at the horizontal resolution of T42 (128x64 grid cells) and 26 vertical levels.

2.2.1. Lawrence Livermore National Laboratory (LLNL)

IMPACT is a 3D off-line chemistry & aerosol transport model that predicts concentrations in the coupled troposphere and stratosphere. For the work reported here, we have used the meteorological fields generated by the NCAR model (see below) and our full NMHC ozone mechanism that covers both tropospheric and stratospheric species (88 species). The chemical mechanism includes O_3, NO_y, ClO_y, HO_y, BrO_y, OH, PAN, NO_x, CO, CH_4, HNO_3, isoprene, ethane, propane, various ketones and aldehydes, and their products. The mechanism is based on *Lurmann et al*. [1986] with various modifications. It is fully described in *Rotman et al*. [2004]. The absorption cross-sections and reaction rate coefficients follow *DeMore et al*. [1997] and *Sander et al*. [2000]. Photolysis is based on a clear sky look-up table using the methodologies from *Douglass et al*. [1997]; rates are adjusted for clouds. The chemical equations are solved using the Gear solver (SMVGEAR II) of *Jacobson* [1995].

The IMPACT model uses the operator splitting technique for emissions, advection, diffusion, convection, deposition, gravitational settling, photolysis, and chemistry. Advection is based on a version of the *Lin and Rood* [1996] scheme, and uses a pressure-fixer scheme to ensure conservation of tracer mass [*Rotman et al*., 2004]. Diffusion is based on the implicit scheme of *Walton et al.* [1988]. Convection is based on the CONVTRANS algorithm of *Rasch et al.* [1997]. Wet-deposition of species is based on

their Henry's law coefficient, and is handled separately for scavenging within convective updrafts, the rest of the convective system, and stratiform clouds. Our scheme is based on *Giorgi and Chameide*s [1986], *Balkanski et al.* [1993] *Mari et al.* [2000] and *Liu et al.* [2001]. Dry-deposition uses the resistances in series approach based on *Wesely et al*. [1985, 1989] and *Wang et al*. [1998]. Gravitational settling of particles is based on *Seinfeld and Pandis* [1998]. The 2000 emissions used for this work came from Granier et al. [2004], except for NO_x from lightning and aircraft, and CH_4, for which we used our standard 1990s emissions [*Rotman et al*., 2004] for both 2000 and 2100.

2.2.2. Max-Planck Institute for Chemistry (MPIC)

The global offline Model of Atmospheric Transport and Chemistry – Max Planck Institute for Chemistry version 3.2 (MATCH-MPIC) is described and evaluated in *Rasch et al*. [1997], *Mahowald et al*. [1997a,b], *Lawrence et al*. [1999], *von Kuhlmann et al*. [2003a,b], *Lawrence et al*. [2003] and references therein.

The meteorology component of MATCH-MPIC simulates advective transport [*Rasch and Lawrence*, 1998], convection [*Zhang and McFarlane*, 1995; *Hack*, 1994], vertical diffusion [*Holtslag and Boville*, 1993], cloud fractions [*Slingo*, 1987], and cloud microphysics [*Rasch and Kristjánsson*, 1998]. Gridded values for basic meteorological parameters (pressure, temperature, horizontal winds, surface heat fluxes, and surface stresses) are obtained from the NCAR Community Atmospheric Model (CAM) simulations (see below). The remaining meteorological properties (e.g. convective cloud transport) are diagnosed online within MATCH-MPIC. MATCH-MPIC has a full tropospheric hydrological cycle; the surface source of water vapor is computed from the latent heat flux in the NCEP data, and the moisture transport and precipitation are

computed using the algorithms in MATCH-MPIC. This gives a water vapor distribution which is internally consistent with the model's meteorology.

For both the 2000 case and the 2100 case, the model was initialized with mean trace gas fields from *von Kuhlmann et al*. [2003a], with a 4 month spin-up for the chemical fields. The photochemical scheme includes a parameterization of non-methane hydrocarbon (NMHC) oxidation covering up to C5 molecules (especially isoprene), and sub-gridscale transport and the hydrological cycle are diagnosed online. Further details can be found via http://www.mpch-mainz.mpg.de/~lawrence.

2.2.3. National Center for Atmospheric Research (NCAR)

The MOZART-2 chemistry-transport model was originally developed at the National Center for Atmospheric Research, the Geophysical Fluid Dynamics Laboratory and the Max-Planck Institute for Meteorology to study tropospheric chemistry. For a complete description of the model and its evaluation, the reader is referred to *Horowitz et al.* [2003] and references therein.

MOZART-2 provides the distribution of 80 chemical constituents (including some non-methane hydrocarbons) between the surface and the stratosphere. In this study, we use the model at a uniform horizontal resolution of ~ 2.8º in both latitude and longitude. The vertical discretization of the meteorological data (described above) and hence of the model consists of 26 hybrid levels from the ground to ~ 4 hPa. The evolution of species is calculated with a time step of 20 minutes.

Dry deposition velocities are calculated interactively using a resistance-in-series scheme [*Wesely*, 1989; *Walmsley and Wesely*, 1996; *Wesely and Hicks*, 2000]. The calculation of surface resistances uses the vegetation distribution of *Bonan et al.* [2002].

Wet deposition is represented as a first-order loss process within the chemistry operator, with loss rates computed based on the large-scale and convective precipitation rates diagnosed by MOZART-2 [*Rasch et al*., 1997; *Horowitz et al.,* 2003]. Soluble species undergo wet removal by in-cloud scavenging, using the parameterization of *Giorgi and Chameides* [1985] based on their temperature-dependent effective Henry's Law constants. In addition, highly soluble species (such as HNO_3 and H_2O_2) are also removed by below-cloud washout, using the formulation described in *Brasseur et al.* [1998].

The NO_x production by lightning follows the *Price and Rind* [1994] and *Price et al.* [1997] parameterization, as discussed in *Horowitz et al*. [2003]. It is scaled to a specified global annual amount; in our case, we specify this amount to be 5 Tg(N)/year (as in *Gauss et al*. [2003]) and calculated the scaling factor for the 2000 case. The same scaling was then applied to all simulations. The 2000 surface emissions are from *Granier et al*. [2004].

2.3. Summary

All the models used in this study include a representation of nitrogen oxides chemistry, wet deposition and dry deposition. Regarding the chemistry, all models have a reasonable description of the chemistry relevant to nitrogen species; the largest differences arise from the way higher hydrocarbons are handled. The wet depositions schemes are based (using different extensions) originally on the first-order loss scheme devised *Giorgi and Chameides* [1985]. This scheme links the wet removal of soluble species (using an effective Henry's law approach) to the occurrence of precipitation. The dry deposition is parameterized using schemes based on the resistance approach devised

by *Wesely* [1989]. Finally, all modes use a lightning parameterization (a non-surface source of NOx) based on the *Price and Rind* [1994] approach. Therefore, all models are similar in their overall design; however each model will differ from extensions of the original schemes and model specific parameters.

3. Description of simulations

All the models were run for at least 2 years. In order to evaluate the interannual variability of nitrogen deposition, several simulations were extended to a maximum of 10 years. Separate wet and dry nitrogen deposition fields were saved as monthly averages.

The ultimate goal of this study will be to model the impact of nitrogen deposition on the carbon cycle as modeled in the Community Land Model (CLM) [*Bonan et al*., 2002; *Oleson et al*., 2004]; therefore these deposition fields were conservatively interpolated to the CLM T31 grid, on which these experiments will be performed. The analysis presented in this study only uses these regridded fields as it allows for a direct comparison of the various model simulations.

4. Description of the forcings

This section documents the main parameters describing the changes between 2000 and 2100 that are relevant to the discussion of nitrogen deposition.

4.1. Changes in sea-surface temperatures.

In all simulations (including 2000 and 2100 cases), the SST field (Figure 1) comes from previously performed simulations from fully coupled ocean-atmosphere models forced according to the A2 scenario [*Cubasch et al*. 2001]; namely we use the GISS model, the HadCM model, the IPSL model or, for the NCAR-labeled SST, the PCM

model [*Washington et al*., 2000]. To limit the impact of interannual variability, a 10-year average was used to create the 2000 and 2100 SST climatologies. From these climatologies, the ΔSST (2100-2000) was created. The ΔSST from the IPSL simulations was not used by any other model due to time constraints on the project.

The 2100 SST distribution is characterized by an increase of the sub-tropical values by 1-3 ^{o}C, with annual average temperature over 32 ^{o}C over large sections. The GISS model simulates the largest response to the 2100 forcings while NCAR simulates the smallest, reflecting differences in their climate sensitivities [*Cubash et al*., 2001].

Large increases in SST will translate into increases in air temperature and tropospheric water vapor and changes in precipitation location and amount. In addition, lightning location, frequency and intensity are likely to be affected as well. All these factors are in the sensitivity of nitrogen deposition to changes in climate.

4.2. Emission of nitrogen oxides

As mentioned in the Introduction, large changes in the emissions of nitrogen oxides (the only significant source of nitrogen containing compounds) are expected to occur under the A2 scenario. This scenario emphasizes the development of large NO_x sources in the tropical and Asian regions by 2100 [*Prather et al*., 2001].

To illustrate this point, we display in Figure 2 the NCAR surface NO_x emissions (including anthropogenic and natural but neither lightning nor aircraft) for 2000, 2100 and their difference. The largest changes are found over eastern Asia (mostly China) where the emissions are found to increase by a factor of 4 according to the A2 scenario; these changes are from anthropogenic emissions only as no changes in emissions from soils were considered. However significant changes are also set to occur over the already

large sources of Western Europe and North America. In addition, widespread increases are expected to occur over Africa, South America and the Indian subcontinent. Finally point sources from megacities (such as Mexico City and Sao Paulo) are expected to become significant contributors to the global budget of nitrogen. Similar conclusions can be drawn from the other emission inventories used in this study.

Estimates for the globally integrated NO_x sources considered in this study range between 35 and 50 Tg(N)/year for 2000 (see Table 2) and between 98 and 131 Tg(N)/year for 2100. The lightning source contributes an additional 2 to 13.5 Tg(N)/year. Among the models used, the largest sensitivity (a factor of 2) of the NO source from lightning to changing the climate was found for the GISS model using the GISS 2100 SST. On the other hand, the lightning source in the NCAR model shows much smaller sensitivity to changes in the climate, of the order of 30%.

5. Analysis of nitrogen deposition

5.1. Evaluation of present-day results

Realistic representation of wet nitrogen deposition requires the combined accurate simulation of precipitation (location and intensity), soluble nitrogen loading and aqueous uptake. As part of the monitoring of acid rain, extensive networks of wet deposition were built in Western Europe (EMEP) and North America (NADP). Frequent measurements were taken over a long period of time, providing enough data to create climatologies. We use a database of such measurements [*Holland et al.,* 2005] to evaluate the models' ability to reproduce the present-day levels of nitrogen deposition over these two regions. Since all chemical models have different resolutions, the model results and the

measurements (only annual averages are used in this study) are averaged at the T31 CLM resolution (see section 3). Statistical analysis of these data is shown in Table 3.

At the NADP stations (Figure 3a), the models tend to reproduce the range of observed values, with all models showing spatial correlation coefficients larger than 0.75. There is however the indication that, for large observed deposition rates, all models tend to overpredict nitrogen wet removal. On average, the models slightly overestimate the mean deposition rate, slightly underestimate the median, and provide a good description of the geographical variability (indicated by the standard deviation). The average correlation coefficient is 0.83. Overall there is clear indication that the annual deposition rate is quite well reproduced in all simulations over North America.

In the case of EMEP (Figure 3b, note the different scale), most models (except HadCM and NCAR) are characterized by an underestimate at low deposition rates and overestimate at medium to high rates. The highest observed deposition rates are underestimated by all models, regardless of the underlying 2000 SST used. On average, the models provide an underestimate of the observed deposition rate (by approximately 15%), the median (by over 25%), the standard deviation and a correlation coefficient of 0.31.

These fairly poor results contrast with the good simulations over the NADP network described above. The main difference between the two networks is probably their geographical distribution. In North America, most of the sites are in fairly rural settings, away from the main emission centers; on the other hand, this cannot be achieved in Europe due to the overall higher population density. Because of the coarse model grids, the large deposition rates (likely to be downwind from high pollution centers) are

likely to be underestimated. Another possibility is a systematic misrepresentation of precipitation in the models over Europe; however we cannot test this hypothesis because such fields were not saved at the time of the simulations.

Over Asia, there is no nitrogen deposition climatology available yet. There is however an East Asia acid deposition network (EANET, see www.adorc.gr.jp/eanet.html) that provides observations, albeit for 2001 only. To compare with our model results, we have used only the rural and remote stations, for a total of 25 stations covering Eastern Asia (namely China, Japan, Mongolia, Republic of Korea and the Asian portion of the Russian Federation for the northeast sector and Indonesia, Malaysia, Philippines, Thailand and Vietnam for the southeast sector). Results are displayed in Figure 3c and summarized in Table 3. All models tend to provide a reasonable description of the low deposition rates but underestimate the higher ones. Indeed, the models seem to only produce deposition rates smaller than 0.4 gN/m^2/year while observed values go up to 0.8 gN/m^2/year. It must however be remembered that we are here comparing T31 aggregated model results with a limited number of point observations. On average, the correlation coefficient is close to 0.6, but with a significant underestimate of the mean and median deposition rate.

5.2. Global distribution of nitrogen deposition in 2000 and 2100

In this section, we discuss the large-scale annual distribution of nitrogen deposition over land-areas for present-day and 2100 conditions. In order to focus our analysis to the land areas only (since we are targeting the impact on the land carbon cycle), we have explicitly set the deposition rates over the ocean to 0 in Figure 4.

In the present-day simulations (Figure 4a) the maximum deposition rates over land are between 1.2 and 1.5 gN/m^2/year. Depending on the model, these values are found over Western Europe and/or China. In all simulations, the Eastern United States is characterized by deposition rates of approximately 1 gN/m^2/year; in addition, the nitrogen deposition over Europe (similar in amplitude to the Eastern United States) extends from the source region in Western Europe all the way to the Ural Mountains (120^oW). Because the GISS emissions for 2000 are considerably smaller than the other models (see Table 3), the large deposition rates over Asia and India are not found in their simulations.

To summarize the model-model variability, we define a relative standard deviation of nitrogen deposition as the standard deviation (among models) of the annual deposition rate over each grid point divided by the mean deposition rate. Over most of the industrialized regions, this standard deviation is less than 45% (as the average interannual variability is of the order of 10% at the most (not shown), many of these features are nevertheless statistically significant); on the other hand, the rest of the world exhibits standard deviations as high as 90%, even where significant deposition occurs. This seems to be mostly due to a large variability in the biomass burning emissions of nitrogen species (mostly NO), especially over South America. As a consequence, the normalized standard deviation among model results is largest over the tropical regions. The analysis of the GISS simulations shows only a slight dependence on the various SST fields; this can be expected, as the present-day SST fields from the various climate models are quite similar (not shown).

In the case of the 2100 simulations (Figure 4b), the dominant feature is the large increase over Asia (from India to China), with more than a tripling of the present-day

deposition rates, in agreement with the expected changes in NO_x emissions (see section 4.2). Significant growth is also expected over the already heavily deposited regions of Europe and North America; in particular, model results (except for GISS) indicate a large increase of nitrogen deposition over western Russia. Also, two models (MPIC and IPSL) indicate a large increase over North Africa, including Saudi Arabia. There is also indication that the rate of increase will be slightly larger over the Eastern United States than over Europe. On the annual timescale, the standard deviation is in most places less than 60%; interestingly, there seems to be less inter-model variability in 2100 than in 2000. This is probably due to the increase of the "well-defined" anthropogenic emissions compared to less-constrained natural (soils and biomass burning) emissions.

5.3. Regional and global, wet and dry deposition

In this section, we discuss the nitrogen deposition over land in terms of regional and global aggregates. Four regions are defined: Asia (60°E to 150°E, 0°N to 75°N), Europe (15°W to 45°E, 35°N to 75°N), North America (135°W to 45°W, 25°N to 75°N) and the globe. For each region, the annual integrated amount of nitrogen deposition over land is calculated, for both wet and dry processes. In addition, we separate the role of wet and dry deposition by displaying the ratio of these quantities. While the underlying land area does not respond differently to dry versus wet deposition of nitrogen, this information gives insight into which process is responsible for the spread in the model results and an indication of their sensitivity to climate change.

At the global scale (Figure 5), the nitrogen deposition over land increases from 30 Tg(N)/year to approximately 80 Tg(N)/year between 2000 and 2100. As indicated by the linear relationship (fitted using a least-square analysis of all the model results), the total

nitrogen deposition correlates quite well with the total nitrogen emissions (including lightning, see Table 2). This linear fit implies that, overall, most models deposit the same proportion of nitrogen emissions. It is however important to note that there are significant deviations from this linear fit; indeed, while the total emissions are quite similar between the GISS and the MPIC 2100 simulations, there is approximately a 30% difference in the estimates of nitrogen deposition. In all regions, the emission-deposition correlation is much tighter for wet deposition than for dry deposition, which has significant outliers. In addition, there is indication that the ratio of dry deposition to wet deposition is likely to increase between 2000 and 2100, except for the GISS model; this relative increase in dry deposition implies that observational networks (in which the wet deposition is explicitly measured and the dry deposition inferred) will underestimate the increase in nitrogen deposition. For all models, the rate of increase of nitrogen deposition is less than the increase in the emissions (as indicated by the 0.7 slope); this imbalance is compensated by an increase in oceanic deposition (see section 5.4) as models are at steady-state or close to it.

Over North America, there is no consensus among models on which process will drive the near doubling of deposition rate; indeed this region has the largest spread for the ratio of dry *versus* wet deposition. Over this region the Hadley model exhibits a much lower wet deposition than any other model. This is true for both present-day and future conditions. This bias comes from a significantly lower deposition rate over the Western United States, while the Eastern portion is quite well simulated (see Figure 3a and Table 3). Over Europe, there is little modification to the dry/wet deposition rates between present-day and 2100. The relative increase in total deposition is very similar to the

North American region, i.e. a near doubling. Finally, over Asia, by 2100, the amount of deposition corresponds to slightly less than half (from approximately one third) of the global nitrogen deposition over land. The ratio of dry *versus* wet deposition is more compact than for the other regions, especially in 2000.

5.4. Deposition on separate ecosystems

In this section, we document the deposition on a set of ecosystems, namely agriculture, bare soil, grass, forest and ocean. Because the impact of nitrogen deposition is very ecosystem dependent [*Townsend et al*., 1996; *Waldrop et al*., 2004], this analysis identifies the amount of nitrogen deposition that each ecosystem receives (Figure 6). In this figure, we compare the average nitrogen deposition rate (in $gN/m^2/year$) over a specific ecosystem (abscissa) to the average nitrogen deposition rate over all land masses. In addition, a linear fit is calculated using the modeled nitrogen deposition rates for the present-day emissions. Deviation from this linear relationship for 2100 emissions indicates that agriculture, grass and forest land areas are expected to receive proportionally a smaller fraction of the 2100 nitrogen emissions than under present-day conditions. In contrast, the rate for bare soils and ocean is going to increase proportionally faster than the total deposition. This effect seems to be slightly reinforced when climate change is considered (not shown). It must be noted that this analysis is only valid for the CLM land cover map and that no changes in land cover between 2000 and 2100 are considered here.

In terms of nitrogen-carbon coupling, it is mostly the forested areas that can contribute significantly to a long-term potential carbon sink as it is characterized by a high C:N ratio and a slow turnover time [*Townsend et al*., 1996]. In this analysis, we

found that, over the forested areas, the average nitrogen deposition rate is expected to increase from a global average of 0.15 (0.12-0.22) gN/m^2/year to 0.42 gN/m^2/year (0.3-0.54). In terms of integrated amounts, the mean values translate respectively to 10 TgN/year and 28 TgN/year. If no saturation takes place, this implies that approximately 3 times as much carbon can be uptaken by the forested areas in 2100 compared to present-day conditions.

5.5. Impact of climate change only

As shown in previous sections, large changes in nitrogen deposition are expected to occur by 2100 as a result of changes from emissions and from climate (precipitation, temperature, water vapor and transport). In this section, we try to identify the fraction due to climate change only. For this purpose, a set of simulations with 2100 climate and 2000 emissions (or *vice versa*) were performed (see Table 1). The sensitivity is calculated as the relative difference (expressed in %)

$$\frac{\text{Ndep}(2100) - \text{Ndep}(2000)}{\text{Ndep}(2000)}$$

where Ndep is the total wet and dry nitrogen deposition over land, annual average for the considered climate states (2100 and 2000). This ratio was calculated from simulations using either 2000 or 2100 emissions.

From the available model simulations (Figure 7, see Table 1) the relative nitrogen deposition change due to climate change alone ranges from a positive increase only (GISS model with the GISS SSTs) to a very mixed signal as in the HadCM model. Except for the decrease over the Western coast of South Africa, there seems to be very little consensus between models on what is the sensitivity of nitrogen deposition to

climate. This is true even when the same SST perturbations are used to drive the climate. As the average interannual variability is of the order of 10% at the most (not shown), many of the features due to climate change alone are statistically significant.

From the analysis of the GISS2 simulations, there is not much difference in the sensitivity to climate whether 2000 or 2100 emissions are used. From these simulations, only small regional changes are found while the large-scale patterns are almost identical.

In addition, since the NO lightning source is climate dependent, the NCAR model performed complementary simulations in which this source was removed. In this case, the removal of the lightning source does very little to the overall results. This is however not surprising since the lightning source in the NCAR model indicates a small absolute sensitivity (from 2 Tg/yr to 2.8 Tg/yr) from climate changes. To the contrary, a large fraction of the increase in the GISS model over the tropics is due to increased lightning activity. Similarly, the large decrease over South America in the HadCM model is associated with an anomalous drying; this has the consequence of reducing wet removal and decreasing the lightning source. Overall, this analysis indicates that wet deposition is the main deposition process affected by climate change. Consequently, models which have a propensity to simulate the nitrogen deposition through dry processes are likely to display a lower sensitivity to climate change.

6. Discussion and conclusions

We have used a multi-model approach to analyze the distribution and amplitude of nitrogen deposition over land under present-day and 2100 conditions. In addition to a variety of models, various sets of emissions and climate conditions were used to span a wider range of possible states. The purpose of creating such a large ensemble is that the

simulated range of results provides a lower bound for the overall uncertainty in the nitrogen deposition rates.

Under present-day conditions, the results form this study show that the integrated deposition over land ranges between 25 and 40 Tg(N)/year. By 2100, under the A2 scenario, the deposition over land is expected to range between 60 and 80 Tg(N)/year. For most models, the deposition over land amounts to approximately 70% of the total nitrogen emitted (from surface sources and lightning) regardless of the climate state or the amount of nitrogen emissions. The remainder is deposited over the oceans.

While models tend to produce similar deposition amounts over land for a given set of emissions, the split between dry and wet deposition rates is very model-dependent. In addition, there is indication that dry deposition over land will increase slightly faster than wet deposition between 2000 and 2100, most likely from increased rapid deposition in the vicinity of the large source areas.

Using the nitrogen emissions from the A2 scenario (usually considered the worst-case scenario), we have found that climate change only plays a minor role (a maximum of 50% from climate change versus a 2-3 fold increase from emissions) in the modeled nitrogen distribution in 2100. Indeed, a result from this analysis is the existence of a strong linear relationship between nitrogen emissions and nitrogen deposition, especially for the 2000 conditions. This linear correlation indicates that most models deposit the same proportion of nitrogen emissions. However, while the linear scaling between emission and deposition rates is likely to still be valid, the role of climate change could become more prominent under less drastic nitrogen emissions.

It was also shown that, using the CLM land cover map and without consideration of land-use changes, agricultural, grassy and forest areas are expected to receive a similar increase in their deposition rate; this increase is however slower than the increase of the average nitrogen deposition over land. On the other hand, bare soils and ocean will receive proportionally more in 2100 than in 2000. Over the forested areas, the average nitrogen deposition rate is expected to increase from 0.15 (0.12-0.22) gN/m^2/year to 0.42 gN/m^2/year (0.3-0.54). In terms of integrated amounts, this translates respectively to 10 TgN/year and 28 TgN/year.

It is clear that the analysis presented in this paper only pertains to the nitrogen emitted as NO or NO_2. However, analysis from two models in which ammonia emissions and chemistry were considered indicates a similar response of ammonia and ammonium nitrate deposition to changes in emissions.

This analysis of a possibly important chemistry-climate interaction can be seen as the first step towards a comprehensive Earth system modeling approach to climate change. We will discuss the implications on the carbon cycle in a follow-up paper.

Acknowledgments. We would like to thank T. Holloway for bringing to our attention the EANET deposition data. L. Emmons and C. Nevison provided constructive comments on an earlier version of this manuscript. Funding for the 2003 and 2004 SANTA FE workshops were provided by CCSM and ACD. Participants to those workshops but who did not directly contribute to this paper are also thanked for the valuable participation in the discussions. JFL was supported by the SciDAC project from the Department of Energy. The National Center for Atmospheric Research is operated by the University Corporation for Atmospheric Research under sponsorship of the National Science Foundation. This paper is dedicated to the memory of my father.

References

Balkanski, Y. J., D. J. Jacob, G. M. Gardner, W. C. Graustein, and K. K. Turekian, "Transport and residence times of tropospheric aerosols inferred from a global three-dimensional simulation of 210Pb", *J. Geophys. Res*., 98, 20,573-20,586, 1993.

Bonan, G. B., et al., The land surface climatology of the Community Land Model coupled to the NCAR Community Climate Model. *J. Clim.*, **15**, 3123–3149, 2002.

Brasseur, G. P., et al., MOZART: A global chemical transport model for ozone and related chemical tracers, 1, Model description. *J. Geophys. Res*., 103, 28,265-28,290, 1998.

Collins,W. D., P. J. Rasch, B. E. Eaton, B. Khattatov, J.-F. Lamarque, and C. S. Zender, Simulating aerosols using a chemical transport model with assimilation of satellite aerosol retrievals: Methodology for INDOEX. *J. Geophys. Res.*, **106**, 7313–7336, 2001.

Collins, W. D., et al., The Community Climate System Model, Version 3. *J. Clim.*, submitted, 2004a.

Collins, W. D., J. M. Lee-Taylor, D. P. Edwards, and G. L. Francis, Effects of increased near-infrared absorption by water vapor on the climate system. Submitted to *J. Geophys.Res.*. , 2004b.

Cubasch et al., Projections of future climate change, in Climate Change 2001, Cambridge University Press, 2001.

DeMore, W. B., S. P. Sander, D. M. Golden, R. F. Hampson, M. J. Kurylo, C. J. Howard, A. R. Ravishankara, C. E. Kolb, and M. J. Molina, "Chemical kinetics and photochemical data for use in stratospheric modeling", JPL Publ., 97-4, 1997.

Douglass, A., R. B. Rood, S. R. Kawa, and D. J. Allen (1997), "A three dimensional simulation of the evolution of the middle latitude winter ozone in the middle stratosphere", *J. Geophys. Res*., 102, 19,217-19,232.

Folberth, G., D. Hauglustaine, J. Lathiµere, and F. Brocheton, Impact of biogenic hydrocarbons on tropospheric ozone; results from a global chemistry-climate model, in preparation, 2004.

Granier, C. et al., Present and future surface emissions of atmospheric compounds, European Commission report EVK 2199900011, 2004.

Gauss, M., et al., Radiative forcing in the 21st century due to ozone changes in the troposphere and the lower stratosphere, *J. Geophys. Res*., 108 (D9), 4292, doi:10.1029/2002JD002624, 2003.

Gedney, N., Cox P.M., and Huntingford C. Climate feedback from wetland methane emissions. Submitted to *Geophys. Res. Lett*., 2004.

Giorgi, F., and W. L. Chameides, "Rainout lifetimes of highly soluble aerosols and gases as inferred from simulations with a general circulation model", *J. Geophys. Res*., 91, 14,367-14,376, 1986.

Guenther, A., et al., A global model of natural volatile organic compound emissions, *J. Geophys. Res.*, *100*, 8873, 1995.

Hack, J. J., Parameterization of moist convection in the National Center for Atmospheric Research community climate model (CCM2), J. Geophys. Res., 99, 5551– 5568, 1994.

Hack, J. J., et al., A slab ocean model. *J. Clim.*, submitted, 2004.

Hauglustaine, D. H., et al., Interactive chemistry in the Laboratoire de Météorologie Dynamique general circulation model: Description and background tropospheric chemistry evaluation, *J.Geophys.Res.*, *109*(D04314), doi:10.1029/2003JD003,957, 2004.

Holland et al., Variations in the predicted spatial distribution of atmospheric nitrogen deposition and their impact on carbon uptake by terrestrial ecosystems, *J. Geophys. Res.*, 102, 15,849-15,866, 1997.

Holland, E.A., B.H. Braswell, J. Sulzman and J.-F. Lamarque, Nitrogen deposition onto the United States and Western Europe: Synthesis of observations and models, *Ecological Applications*, in press, 2005.

Holtslag, A. A. M., and B. A. Boville, Local versus nonlocal boundary layer diffusion in a global climate model, *J. Clim*., 6, 1825– 1841, 1993.

Horowitz, L. W., et al., A global simulation of tropospheric ozone and related tracers: Description and evaluation of MOZART, version 2., *J. Geophys. Res.*, 108(D24), 4784, doi:10.1029/2002JD002853, 2003.

Jacobson, M. A., "Computation of global photochemistry with SMVGEAR II", *Atmos. Environ*., Part A, 29, 2541-2546, 1995.

Jenkinson, D.S., K. Goulding, and D.S. Powlson, Nitrogen deposition and sequestration, *Nature*, 400, 629-629, 1999.

Krinner et al., A dynamical global vegetation model for studies of the coupled atmosphere-biosphere system, *Global Biogeochem. Cycles*, *in press*, 2004.

Lawrence, M. G., Crutzen, P. J., Rasch, P. J., Eaton, B. E., and Mahowald, N. M., A model for studies of tropospheric photochemistry: Description, global distributions, and evaluation, *J. Geophys. Res*., 104, 26 245–26 277, 1999.

Lawrence, M. G. et al., Global chemical weather forecasts for field campaign planning: predictions and observations of large-scale features during MINOS, CONTRACE, and INDOEX. Atmospheric Chemistry and Physics, Vol. 3, pp 267-289, 26-2-2003

Lin, S. J., and R. B. Rood, "A fast flux form semi-Lagrangian transport scheme on the sphere", *Mon. Weather Rev*., 124, 2046-2070, 1996.

Liu, H., D. J. Jacob, I. Bey, and R. M. Yantosca, "Constraints from 210Pb and 7Be on wet deposition and transport in a global three-dimensional chemical tracer model driven by assimilated meteorological fields", *J. Geophys. Res*., 106, 12,109-12,128, 2001.

Logan, J.A., An analysis of ozonesonde data for the troposphere: Recommendations for testing 3-D models and development of a gridded climatology for tropospheric ozone, *J. Geophys. Res.*, *104*, 16,115-16,149, 1999.

Lurmann, F. W., A. C. Lloyd, and R. Atkinson, "A chemical mechanism for use in long-range transport/acid deposition computer modeling*", J. Geophys. Res*., 91, 10,905-10,936, 1986.

Mahowald, N. M., R. G. Prinn, and P. J. Rasch, Deducing CCl3F emissions using an inverse method and chemical transport models with assimilated winds, *J. Geophys. Res*., 102, 28,153– 28,168, 1997a.

Mahowald, N. M., P. J. Rasch, B. E. Eaton, S. Whittlestone, and R. G. Prinn, Transport of 222radon to the remote troposphere using the Model of Atmospheric Transport and Chemistry and assimilated winds from ECMWF and the National Center for Environmental Prediction/NCAR, *J. Geophys*. Res., 102, 28,139– 28,152, 1997b.

Mari, C., D. J. Jacob, and P. Bechtold, "Transport and scavenging of soluble gases in a deep convective cloud", *J. Geophys. Res*., 105, 22,255-22,267, 2000.

Nadelhoffer, K.J., B.A. Emmett and P. Gunderson, Nitrogen deposition makes a minor contribution to carbon sequestration in temperate forests, *Nature*, 398, 145-148, 1999.

Oleson, K. W., et al., Technical description of the Community Land Model (CLM). Technical Report NCAR/TN-461+STR, National Center for Atmospheric Research, Boulder, CO. 80307-3000, 174 pp, 2004.

Ollinger, S.V., J.D. Aber, P.B. Reich, and R.J. Freuder, Interactive effects of nitrogen deposition, tropospheric ozone, elevated CO2 and land use history on the carbon dynamics of northern hardwood forests, *Global Change Biology*, 8, 545-562, 2002.

Olivier et al., Applications of EDGAR. Including a description of EDGAR 3.0: reference database with trend data for 1970-1995, *RIVM report 773301 001*, RIVM, 2001.

Penner, J.E., C.S. Atherton, and T.E. Graedel, Global emissions and models of photochemically active compounds, in Global Atmospheric Biospheric Chemistry, ed R.G. Prinn, Plenum, New York, 1994.

Prentice, M. J. et al., The carbon cycle and atmospheric carbon dioxide, in Climate Change 2001, Cambridge University Press, 2001.

Prather, M. J. et al., Atmospheric chemistry and greenhouse gases, in Climate Change 2001, Cambridge University Press, 2001.

Price, C., and D. Rind, Modeling global lightning distribution in a general circulation model, *Mon. Weather Rev*., 122, 1930– 1939, 1994.

Price, C., J. Penner, and M. Prather, NO*x* from lightning, 1, Global distribution based on lightning physics, *J. Geophys. Res.*, *102*, 5929-5941, 1997.

Rasch, P.J., N.M. Mahowald, and B.E. Eaton, Representations of transport, convection, and the hydrologic cycle in chemical transport models: Implications for the modeling of short-lived and soluble species, *J. Geophys. Res.*, *102*, 28,127-28,138, 1997.

Rasch, P. J., and J. E. Kristjansson, A comparison of the CCM3 model climate using diagnosed and predicted condensate parameterizations, *J. Clim*., 11, 1587–1614, 1998.

Rasch, P. J.,W. D. Collins, and B. E. Eaton, Understanding the Indian Ocean Experiment (INDOEX) aerosol distributions with an aerosol assimilation. *J. Geophys. Res.*, **106**, 7337–7356, 2001.

Rotman D. A., et al., IMPACT, the LLNL 3-D global atmospheric chemical transport model for the combined troposphere and stratosphere: Model description and analysis of ozone and other trace gases, *J. Geophys. Res..*, 109, D04303, doi:10.1029/2002JD003155, 2004.

Sadourny, R., and K. Laval, January and July performance of the LMD general circulation model, in *New Perspectives in Climate Modeling*, edited by A. Berger and C. Nicolis, pp. 173-197, Elsevier, 1984.

Sander, S. P., et al., "Chemical kinetics and photochemical data for use in stratospheric modeling: Supplement to Evaluation 12: Update of key reactions", Evaluation 13, JPL Publ., 00-003, 2000.

Sanderson, M.G., Collins, W.J., Derwent, R.G. and Johnson, C.E. Simulation of global hydrogen levels using a Lagrangian three-dimensional model. *J. Atmos. Chem*, 46, 15-28, 2003.

Schimel, D. S., Terrestrial ecosystems and the carbon cycle, *Global Change Biology*, 1, 77-91, 1995.

Schmidt, G.A., et al., Present day atmospheric simulations using GISS ModelE: Comparison to in-situ, satellite and reanalysis data, *J. Clim.*, *submitted*, 2004.

Schulze, E.D., W. Devries and M. Hauhs, Critical loads of nitrogen deposition on forest ecosystems, *Water Air and Soil Pollution*, 48, 451-456, 1989.

Seinfeld, J. H., and S. N. Pandis, "Atmospheric Chemistry and Physics", John Wiley, New York, 1998.

Shindell, D.T., G. Faluvegi, and N. Bell, Preindustrial-to-present-day radiative forcing by tropospheric ozone from improved simulations with the GISS chemistry-climate GCM, *Atmos. Chem. Phys.*, *3*, 1675-1702, 2003.

Sievering, H.L., Nitrogen deposition and sequestration, *Nature*, 400, 630-630, 1999.

Slingo, J. M., The development and verification of a cloud prediction scheme for the ECMWF model, *Q. J. R. Meteorol. Soc*., 113, 899– 927, 1987.

Throop, H.L., E. A. Holland, W. J. Paron, D. S. Ojima and C.A. Keough, Effects of nitrogen deposition and insect herbivory on patterns of ecosystem-level carbon and nitrogen dynamics: results from the CENTURY model, *Global Change Biology*, 10, 1092-1105, 2004.

Tiedke, M., A comprehensive mass-flux scheme for cumulus parameterization in large scale models, *Mon. Wea. Rev.*, pp. 1,779{1,800, 1989.

Townsend A.R., B.H. Braswell, E.A. Holland, and J.E. Penner, Spatial and temporal patterns in terrestrial carbon storage due to the deposition of fossil-fuel nitrogen. Ecological Applications, 6, 806-814, 1996.

Van der Werf et al., Carbon emissions from fires in tropical and subtropical ecosystems, *Global Change Biology*, *9*, 547-562,2003.

Van Leer, B., Towards the ultimate conservative difference scheme. Part IV: A new approach to numerical convection, *J. Comp. Phys.*, *23*, 276-299, 1977.

Vitousek, P.M., et al., Human alteration of the global nitrogen cycle: sources and consequences. Ecological Applications, 7, 737-750, 1997.

von Kuhlmann, R., M. G. Lawrence, P. J. Crutzen, and P. J. Rasch, A model for studies of tropospheric ozone and nonmethane hydrocarbons: Model description and ozone results, *J. Geophys. Res*., 108, 4294, doi:10.1029/2002JD002893, 2003a.

von Kuhlmann R., M. G. Lawrence, P. J. Crutzen, P. J. Rasch, A model for studies of tropospheric ozone and nonmethane hydrocarbons: Model evaluation of ozone‐related species, *J. Geophys. Res., 108*, 4729, doi:10.1029/2002JD003348, 2003b.

Waldorp, M. P., D. R. Zak, R. L. Sinsabaugh, M. Gallo, and C. Lauber**,** Nitrogen deposition modifies soil carbon storage through changes in microbial enzymatic activity, *Ecological Applications*, 14, 1172-1177, 2004

Walmsley J.L. and M.L. Wesely, Modification of coded parametrizations of surface resistances to gaseous dry deposition, Atmospheric Environment, 30, 1181-1188, 1996.

Walton, J. J., M. C. MacCracken, and S. J. Ghan, "A global-scale Lagrangian trace species model of transport, transformation, and removal processes", *J. Geophys. Res*., 93, 8339-8354, 1998.

Wang, Y., D. J. Jacob, and J. A. Logan, "Global simulation of tropospheric O3-NOx-hydrocarbon chemistry: 1. Model formulation", *J. Geophys. Res*., 103, 10,713-10,725, 1998.

Washington, W. M., et al., Parallel climate model (PCM) control and transient simulations. *Clim. Dyn.*, 16, 755-774, 2000.

Wesely, M. L., Parameterizations for surface resistance to gaseous dry deposition in regional-scale numerical models, *Atmos. Environ*., 23, 1293-1304, 1989.

Wesely, M. L., and B. B. Hicks, A review of the current status of knowledge on dry deposition, *Atmos. Environ*., **34**, 2261-2282, 2000.

Wesely, M. L., D. R. Book, R. L. Hart, and R. E. Speer, Measurements and parameterization of particulate sulfur dry deposition over grass, *J. Geophys. Res*., 90, 2131-2143, 1985.

Zhang, G. J., and N. A. McFarlane, Sensitivity of climate simulations to the parameterization of cumulus convection in the Canadian Climate Centre general circulation model, Atmos. Ocean, 33, 407– 446, 1995.

Zhang, M., W. Lin, C. B. Bretherton, J. J. Hack, and P. J. Rasch: A modified formulation of fractional stratiform condensation rate in the NCAR Community Atmosphere Model (CAM2). *J. Geophys. Res.*, **108**, DOI 10.1029/2002JD002523, 2003.

Figure 1. Sea-surface temperatures for 2000 (only the one from NCAR is shown) and 2100 used by the various models in this study.

Figure 2. Annual total surface NO_x emissions (in $gN/m^2/year$) for 2000, 2100 and their difference used for the NCAR model. Others models have similar geographical distribution and are therefore not displayed.

Figure 3. Scatter plot of the modeled HNO_3 annual wet deposition rate (in $gN/m^2/year$) *versus* the observed annual wet deposition over (a) North America (NADP network), (b) Western Europe (EMEP network) and (c) Asia (EANET network). Over each plot is the reference to the model used, followed by the SST field used.

Figure 4. Global distribution of the annual average nitrogen deposition rate (in $gN/m^2/year$) over land areas in (a) 2000 and (b) 2100. Each plot is referenced by the model used, followed by the SST field used. In addition, the last two plots are the mean of all the models and its standard deviation (expressed in fraction: a value of 1 corresponds to 100%).

Figure 5. Scatter plot of the integrated nitrogen deposition (in Tg(N)/year) over all land areas (top row), Asia (second row), North America (third row) and Europe (bottom row). The first column shows the results for dry deposition, the second column for wet deposition, the third column for the total and the fourth column for the ratio of dry deposition over wet deposition. In all plots, the horizontal axis is the global emissions (including lightning) for each model. A least-square linear fit is performed independently for each plot in the first 3 columns; the slope is shown for the total deposition only.

Figure 6. Scatter plot of the nitrogen deposition rate (in gN/m2/year) over a variety of ecosystems. A least-square linear fit is performed using the results for the 2000 emissions only.

Figure 7. Global distribution of the relative change (in %) in the annual average nitrogen deposition rate (in $gN/m^2/year$) over land areas from changes in climate. Each plot is referenced by the model used, followed by the SST field used and specifics about the model simulation.

Model	SST	Climate	Emissions	Lightning
GISS1	GISS	2000	2000	x
GISS1	NCAR	2000	2000	x
GISS1	HadCM	2000	2000	x
GISS1	GISS	2100	2000	x
GISS1	NCAR	2100	2000	x
GISS1	GISS	2100	2100	x
GISS2	GISS	2000	2000	x
GISS2	GISS	2000	2100	x
GISS2	GISS	2100	2000	x
GISS2	GISS	2100	2100	x
HadCM	HadCM	2000	2000	x
HadCM	HadCM	2000	2100	x
HadCM	HadCM	2100	2100	x
HadCM	HadCM	2100	2100	
IPSL	IPSL	2000	2000	x
IPSL	IPSL	2100	2100	x
LLNL	NCAR	2000	2000	x
LLNL	NCAR	2100	2100	x
MPIC	NCAR	2000	2000	x
MPIC	NCAR	2100	2100	x
NCAR	NCAR	2000	2000	x
NCAR	NCAR	2000	2000	
NCAR	GISS	2100	2100	x
NCAR	NCAR	2100	2100	x
NCAR	HadCM	2100	2100	x
NCAR	NCAR	2100	2100	
NCAR	NCAR	2100	2000	x
NCAR	NCAR	2100	2000	

Table 1. List of simulations. The crosses in the lightning column indicate the consideration of the NOx lightning source in the simulation.

Model	2000	2100	Lightning
GISS1/2	35	119	6-13.5
HadCM	57	105	NA
IPSL	45	123	5
LLNL	45	118	5
MPIC	37	131	2
NCAR	45	118	2.2-2.8

Table 2. Summary of NO_x emissions (as Tg(N)/year) for year 2000 and 2100, including the range of lightning emissions (for all climate states). Please note that HadCM did not provide the lightning source amount separately.

EMEP	Mean	Median	Std. dev.	Corr. coef.
observations	0.32	0.31	0.21	
GISS1 GISS	0.34	0.28	0.22	0.26
GISS2 GISS	0.38	0.30	0.28	0.26
GISS1 HadCM	0.32	0.26	0.21	0.25
GISS1 NCAR	0.27	0.22	0.17	0.22
HadCM HadCM	0.17	0.17	0.06	0.44
IPSL IPSL	0.29	0.24	0.16	0.38
LLNL NCAR	0.30	0.23	0.17	0.24
MPIC NCAR	0.23	0.22	0.12	0.35
NCAR NCAR	0.25	0.22	0.10	0.29
Models average	0.28	0.24	0.16	0.30
NADP	Mean	Median	Std. dev.	Corr. coef.
observations	0.19	0.20	0.12	
GISS1 GISS	0.23	0.23	0.12	0.85
GISS2 GISS	0.25	0.23	0.15	0.84
GISS1 HadCM	0.20	0.21	0.12	0.85
GISS1 NCAR	0.21	0.20	0.12	0.82
HadCM HadCM	0.20	0.22	0.10	0.87
IPSL IPSL	0.20	0.14	0.14	0.75
LLNL NCAR	0.28	0.19	0.23	0.77
MPIC NCAR	0.19	0.18	0.12	0.86
NCAR NCAR	0.19	0.16	0.13	0.81
Models average	0.21	0.20	0.14	0.83
EANET	Mean	Median	Std. dev.	Corr. coef.
observations	0.26	0.23	0.19	
GISS1 GISS	0.14	0.08	0.10	0.58
GISS2 GISS	0.14	0.07	0.11	0.54
GISS1 HadCM	0.13	0.07	0.09	0.62
GISS1 NCAR	0.13	0.08	0.09	0.62
HadCM HadCM	0.18	0.11	0.09	0.41
IPSL IPSL	0.22	0.09	0.15	0.47
LLNL NCAR	0.17	0.06	0.12	0.59
MPIC NCAR	0.18	0.08	0.12	0.70
NCAR NCAR	0.20	0.11	0.11	0.67
Models average	0.16	0.08	0.11	0.58

Table 3. Summary of comparison of modeled present-day nitrogen deposition with observations over Europe (EMEP), North America (NADP) and Asia (EANET). Units are $gN/m^2/year$.

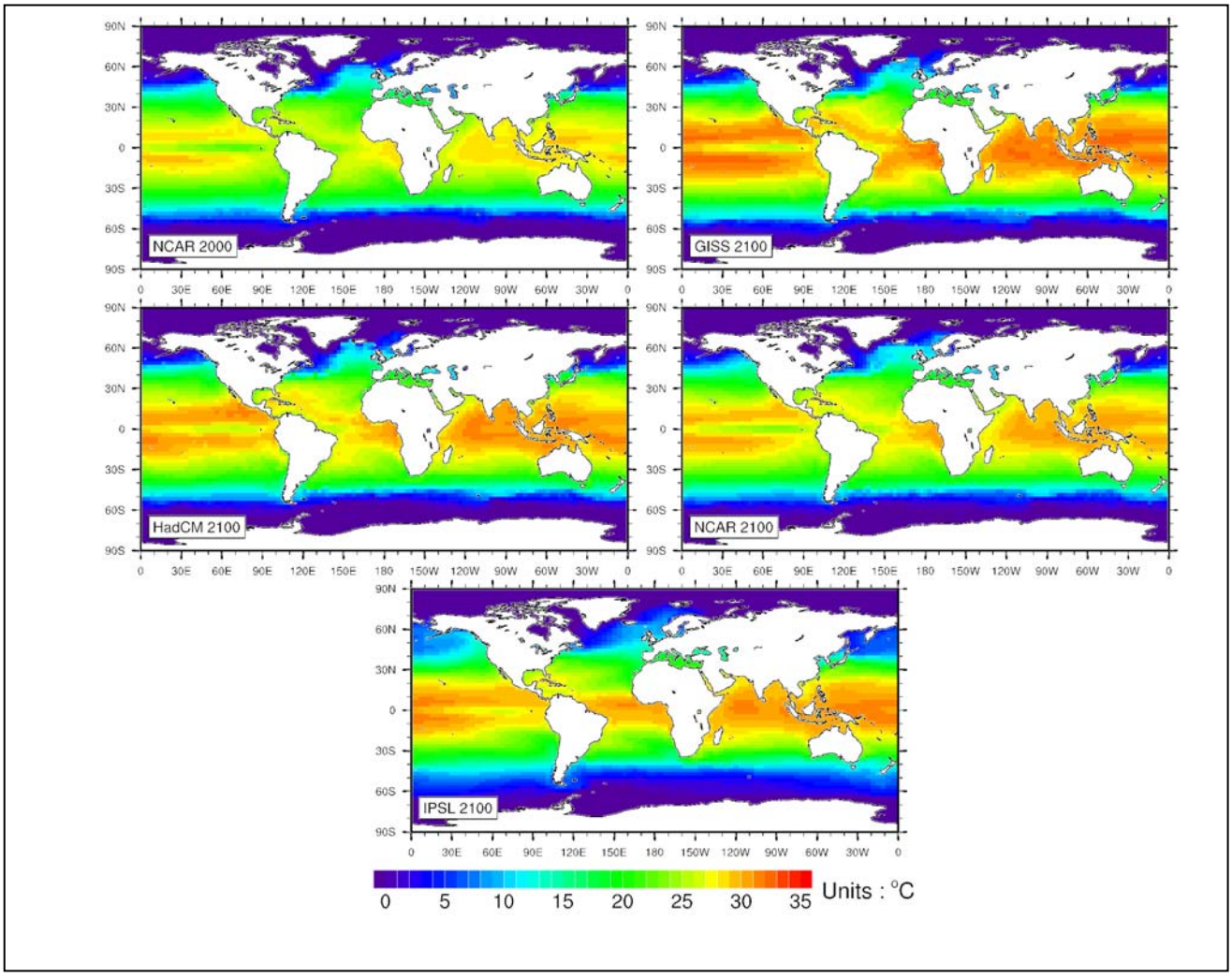
NCAR 2000
GISS 2100
HadCM 2100
NCAR 2100
IPSL 2100
90N
60N
30N
0
30S
60S
90S
0 30E 60E 90E 120E 150E 180 150W 120W 90W 60W 30W 0
0 5 10 15 20 25 30 35
Units : °C

Figure 1

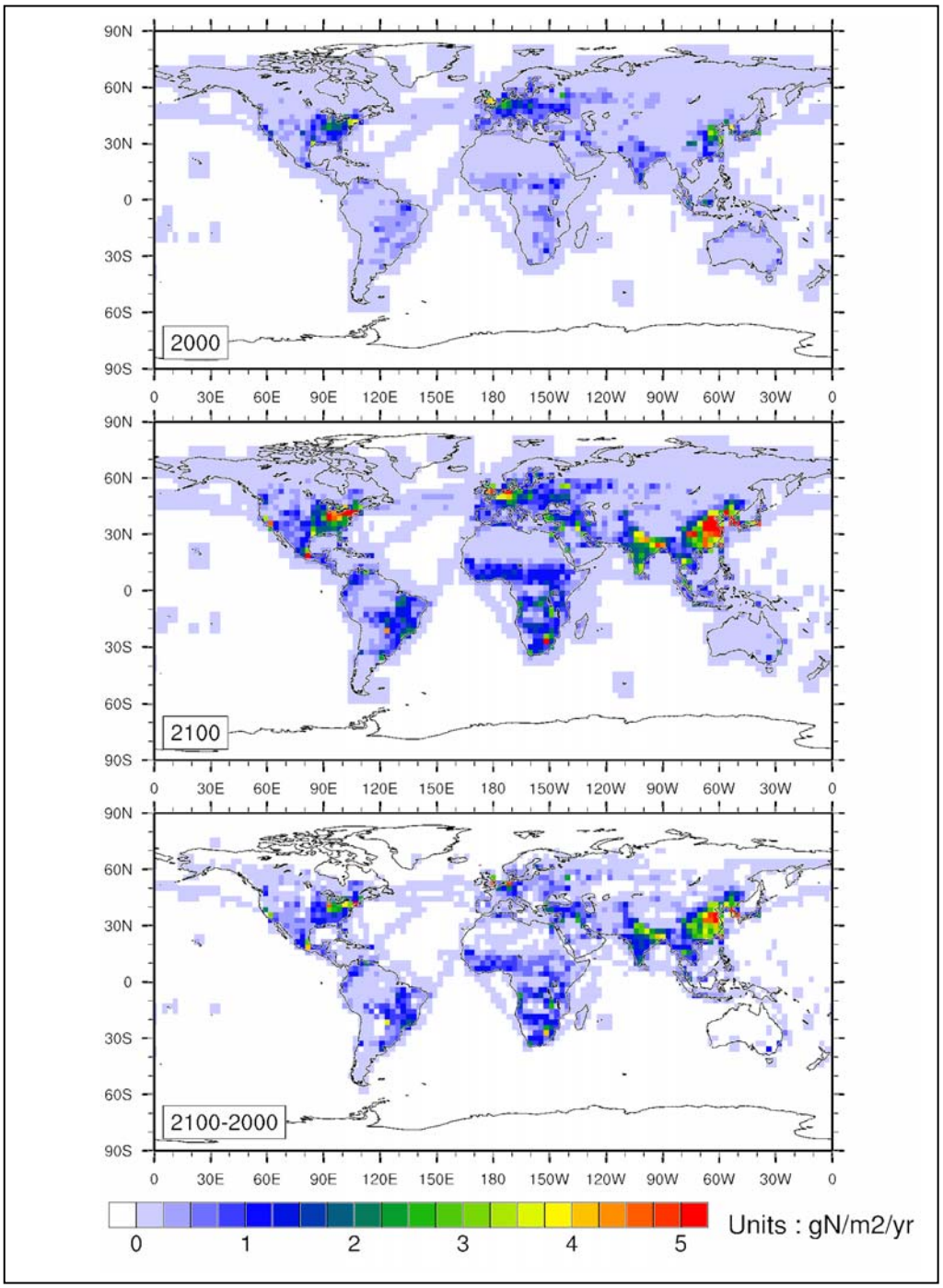
90N
60N
30N
0
30S
60S
90S
2000
0 30E 60E 90E 120E 150E 180 150W 120W 90W 60W 30W 0
2100
2100-2000
0 1 2 3 4 5
Units : gN/m2/yr

Figure 2

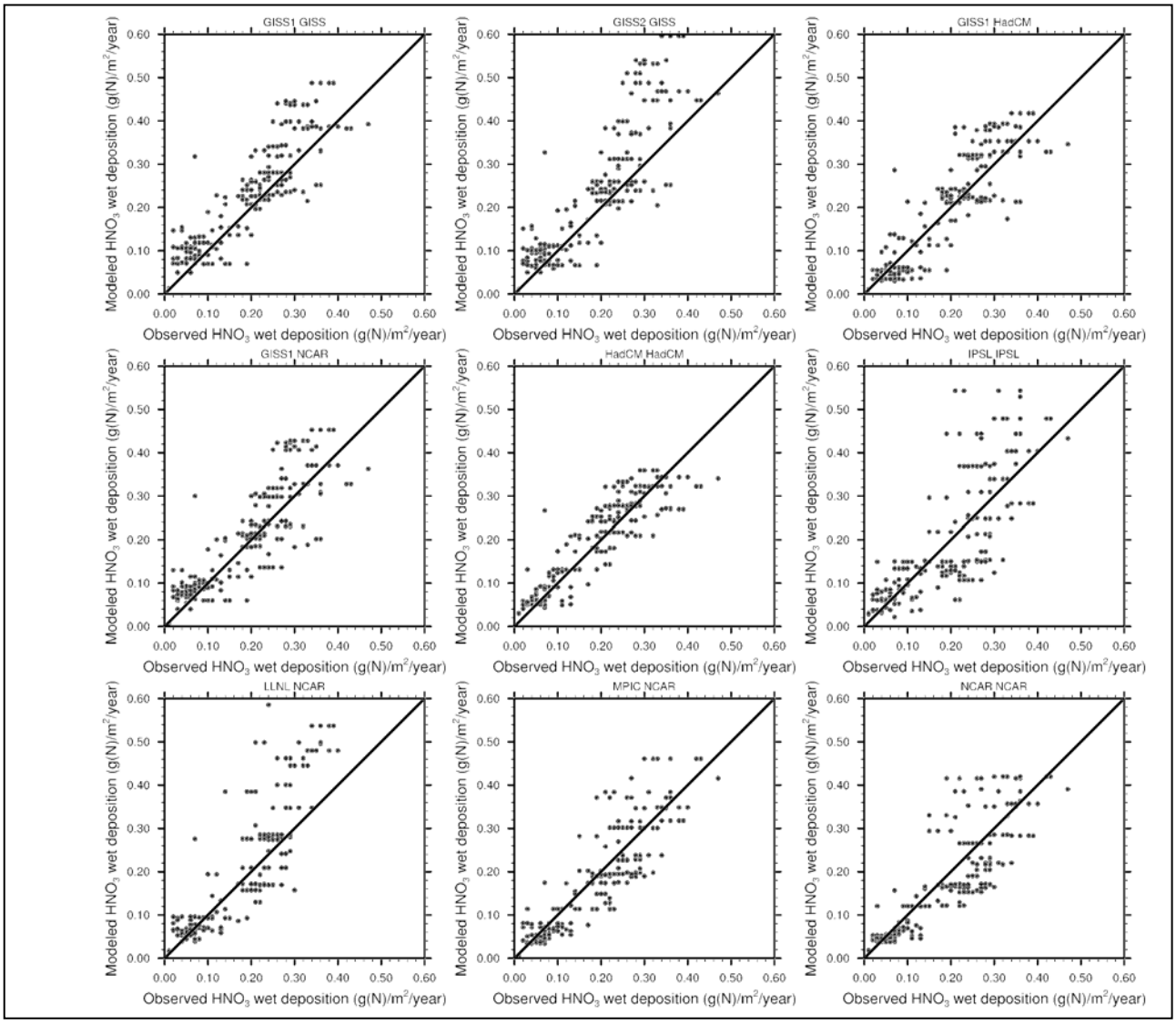
GISS1 GISS
GISS2 GISS
GISS1 HadCM
GISS1 NCAR
HadCM HadCM
IPSL IPSL
LLNL NCAR
MPIC NCAR
NCAR NCAR
Modeled HNO3 wet deposition (g(N)/m2/year)
Observed HNO3 wet deposition (g(N)/m2/year)
0.00
0.10
0.20
0.30
0.40
0.50
0.60

Figure 3a

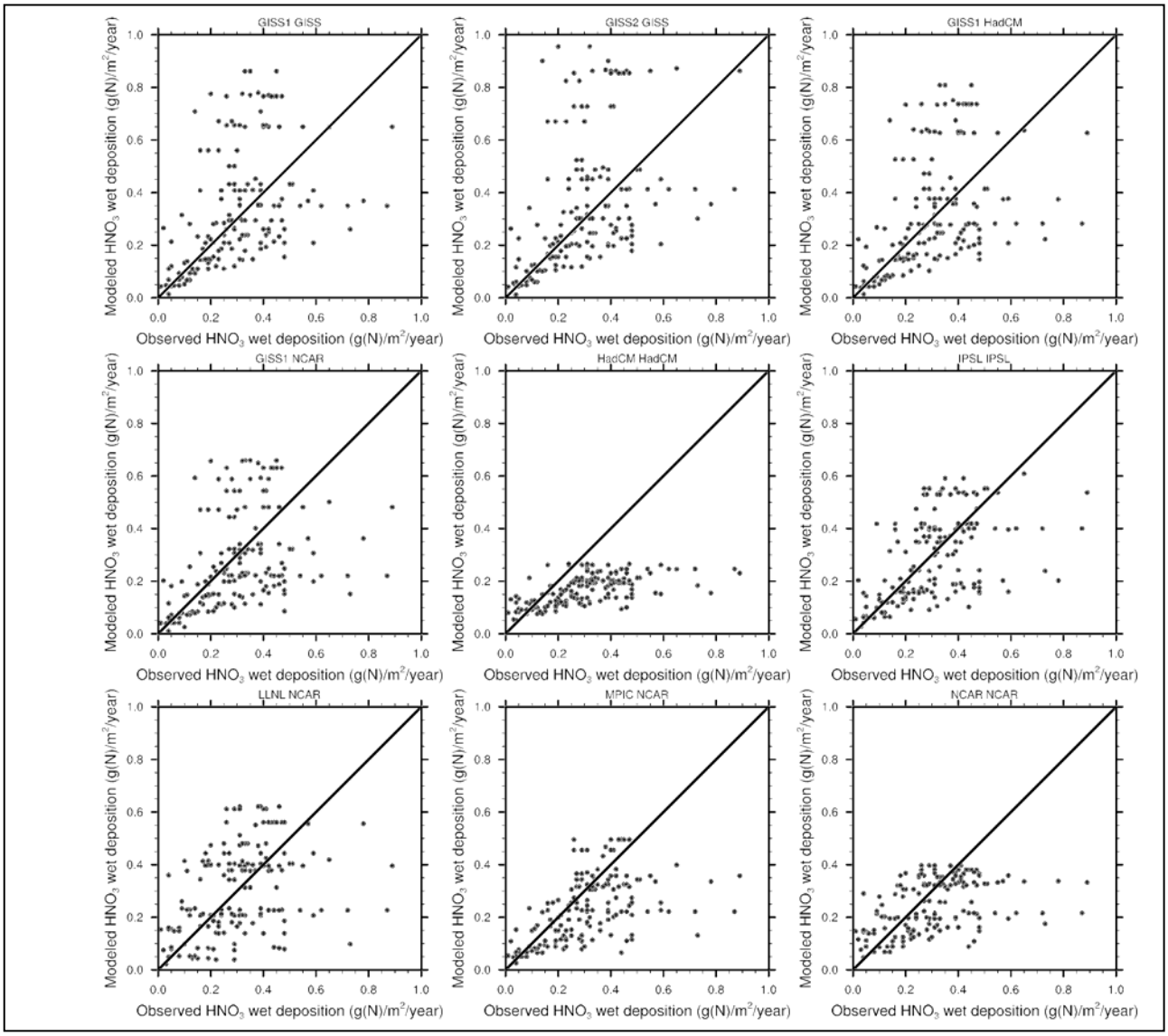
GISS1 GISS
GISS2 GISS
GISS1 HadCM
GISS1 NCAR
HadCM HadCM
IPSL IPSL
LLNL NCAR
MPIC NCAR
NCAR NCAR
Modeled HNO3 wet deposition (g(N)/m2/year)
Observed HNO3 wet deposition (g(N)/m2/year)
0.0
0.2
0.4
0.6
0.8
1.0

Figure 3b

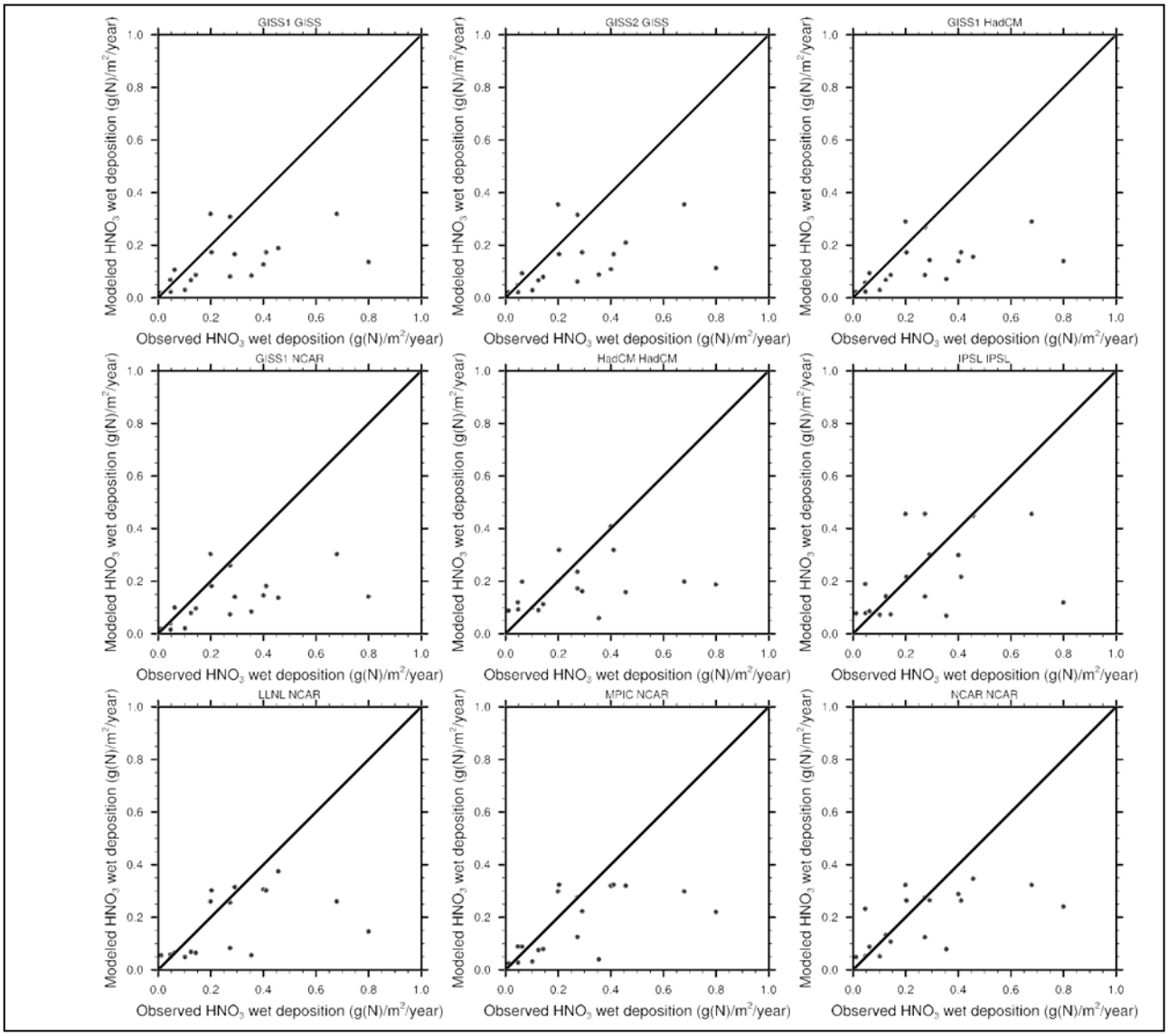
GISS1 GISS
GISS2 GISS
GISS1 HadCM
GISS1 NCAR
HadCM HadCM
IPSL IPSL
LLNL NCAR
MPIC NCAR
NCAR NCAR
Modeled HNO3 wet deposition (g(N)/m2/year)
Observed HNO3 wet deposition (g(N)/m2/year)
0.0
0.2
0.4
0.6
0.8
1.0

Figure 3c

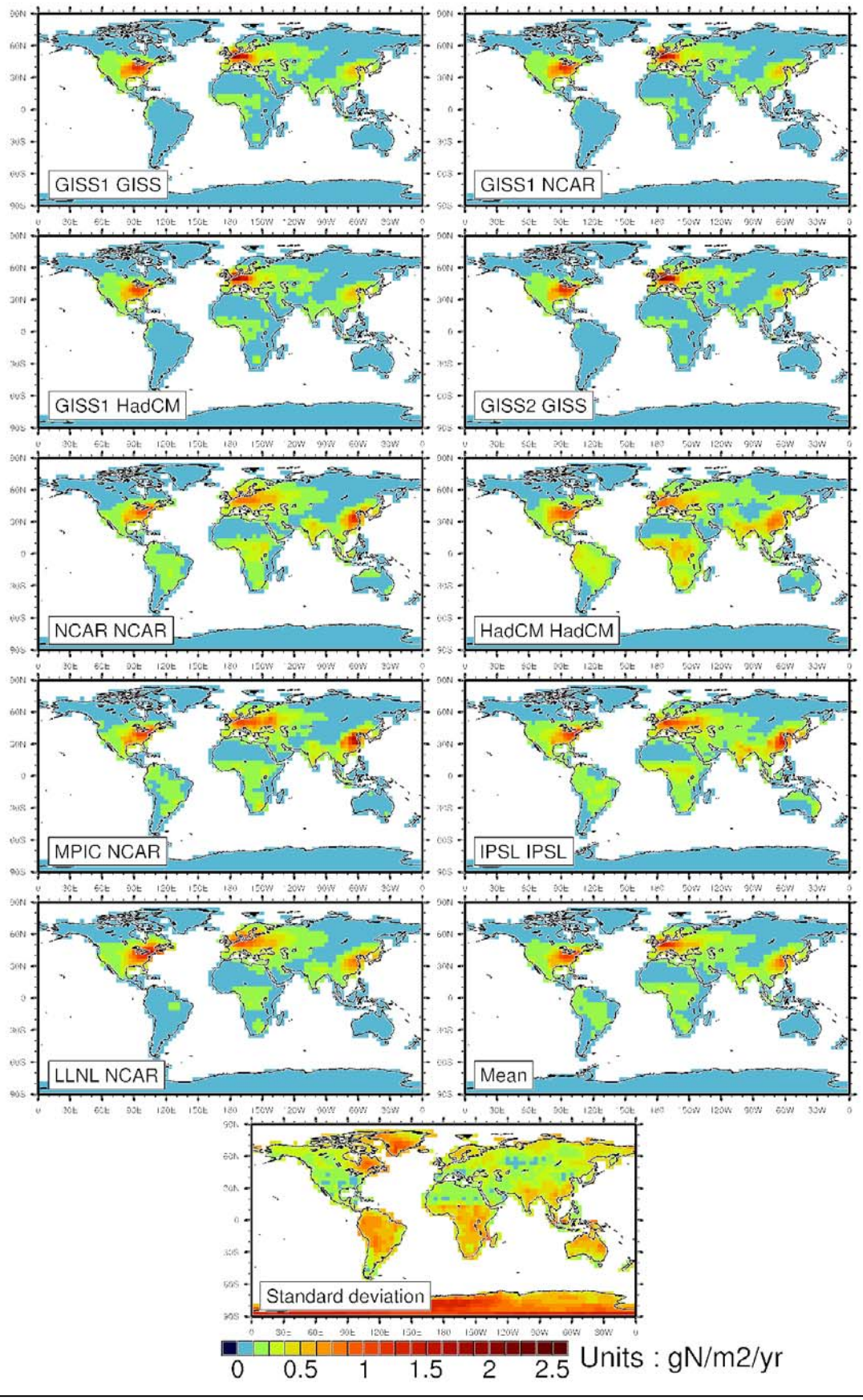
GISS1 GISS
GISS1 NCAR
GISS1 HadCM
GISS2 GISS
NCAR NCAR
HadCM HadCM
MPIC NCAR
IPSL IPSL
LLNL NCAR
Mean
Standard deviation
0
0.5
1
1.5
2
2.5
Units : gN/m2/yr

Figure 4a

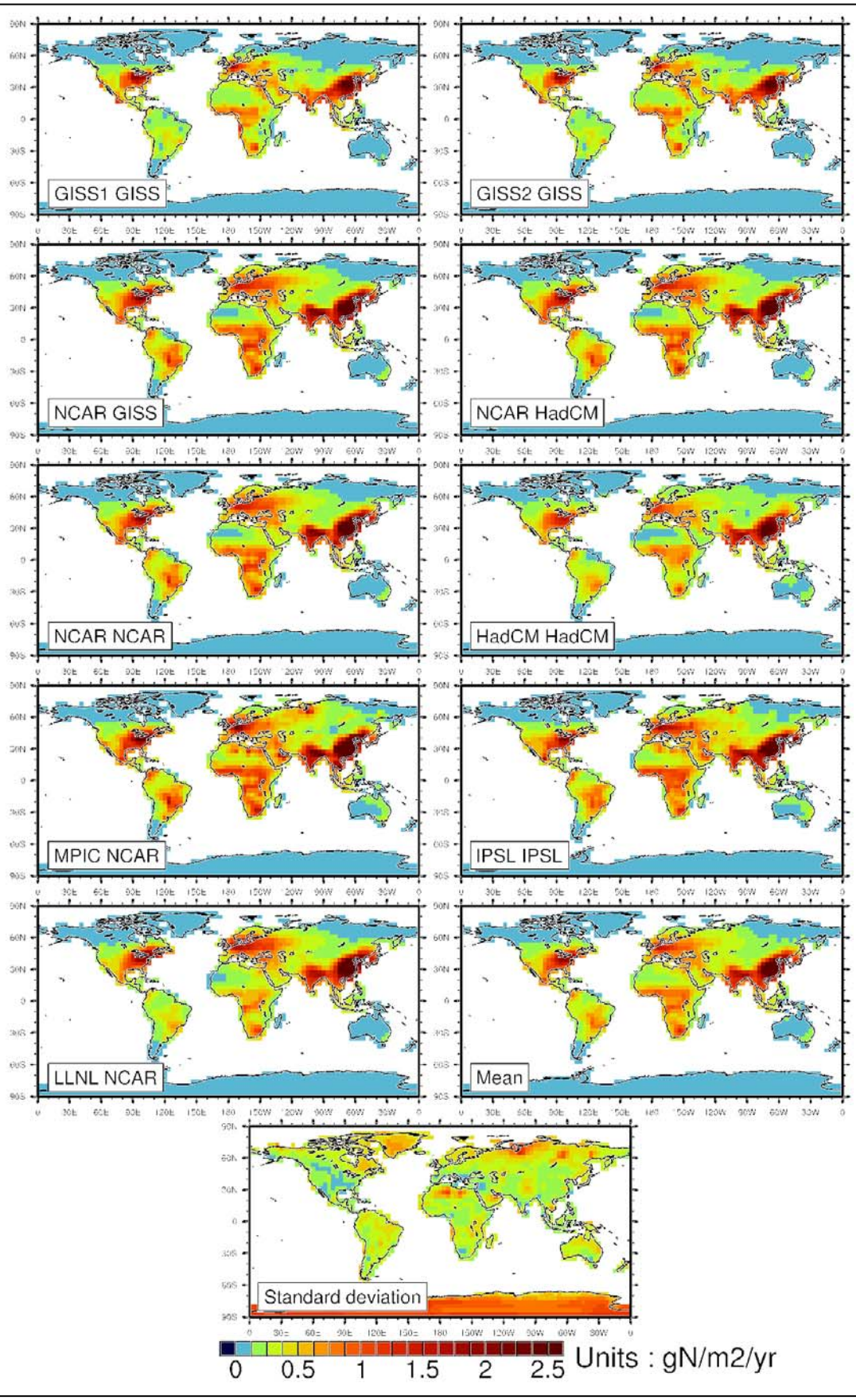
GISS1 GISS
GISS2 GISS
NCAR GISS
NCAR HadCM
NCAR NCAR
HadCM HadCM
MPIC NCAR
IPSL IPSL
LLNL NCAR
Mean
Standard deviation
0
0.5
1
1.5
2
2.5
Units : gN/m2/yr

Figure 4b

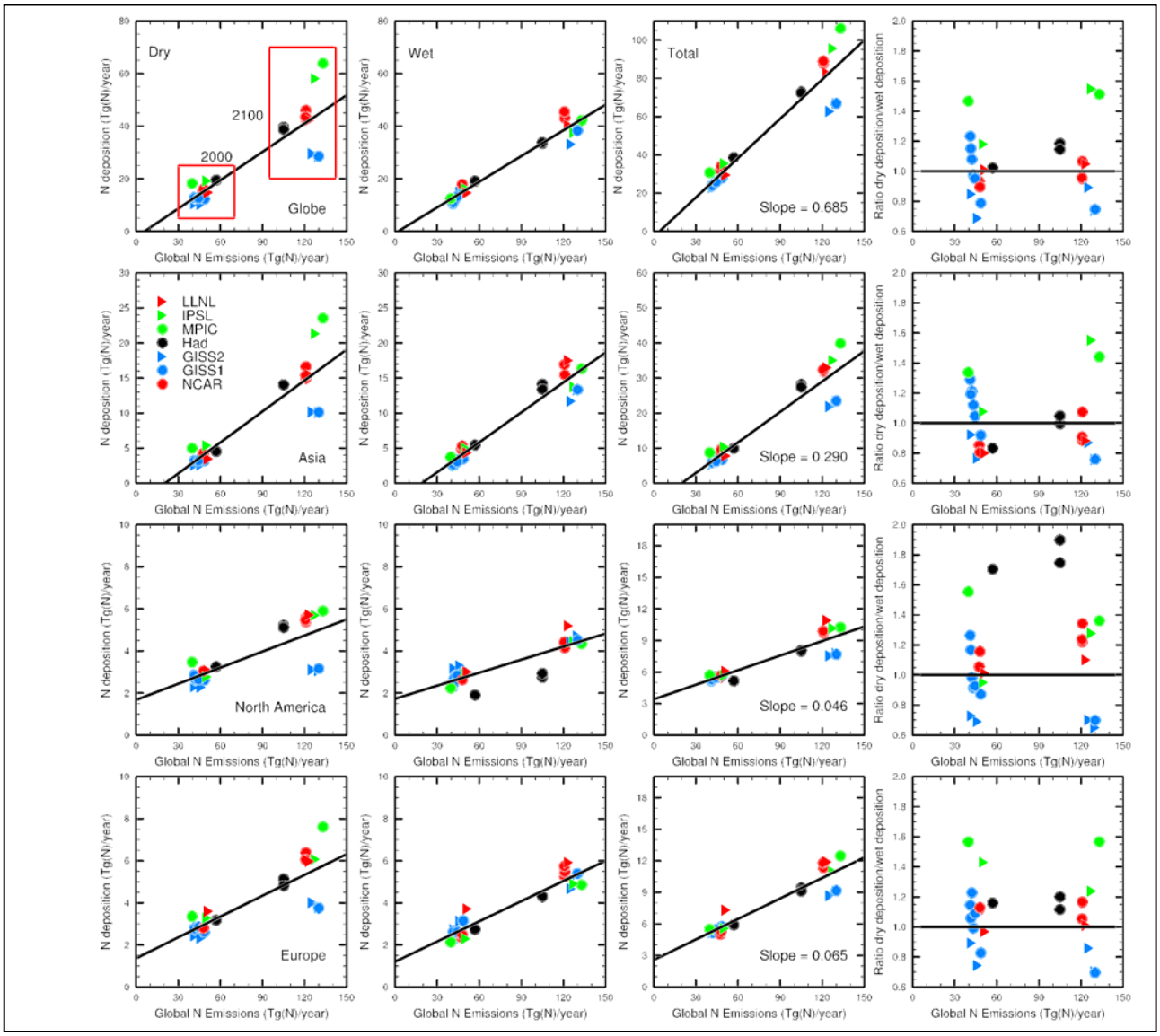
Dry
Wet
Total
2100
2000
Globe
Slope = 0.685
LLNL
IPSL
MPIC
Had
GISS2
GISS1
NCAR
Asia
Slope = 0.290
North America
Slope = 0.046
Europe
Slope = 0.065
N deposition (Tg(N)/year)
Global N Emissions (Tg(N)/year)
Ratio dry deposition/wet deposition

Figure 5

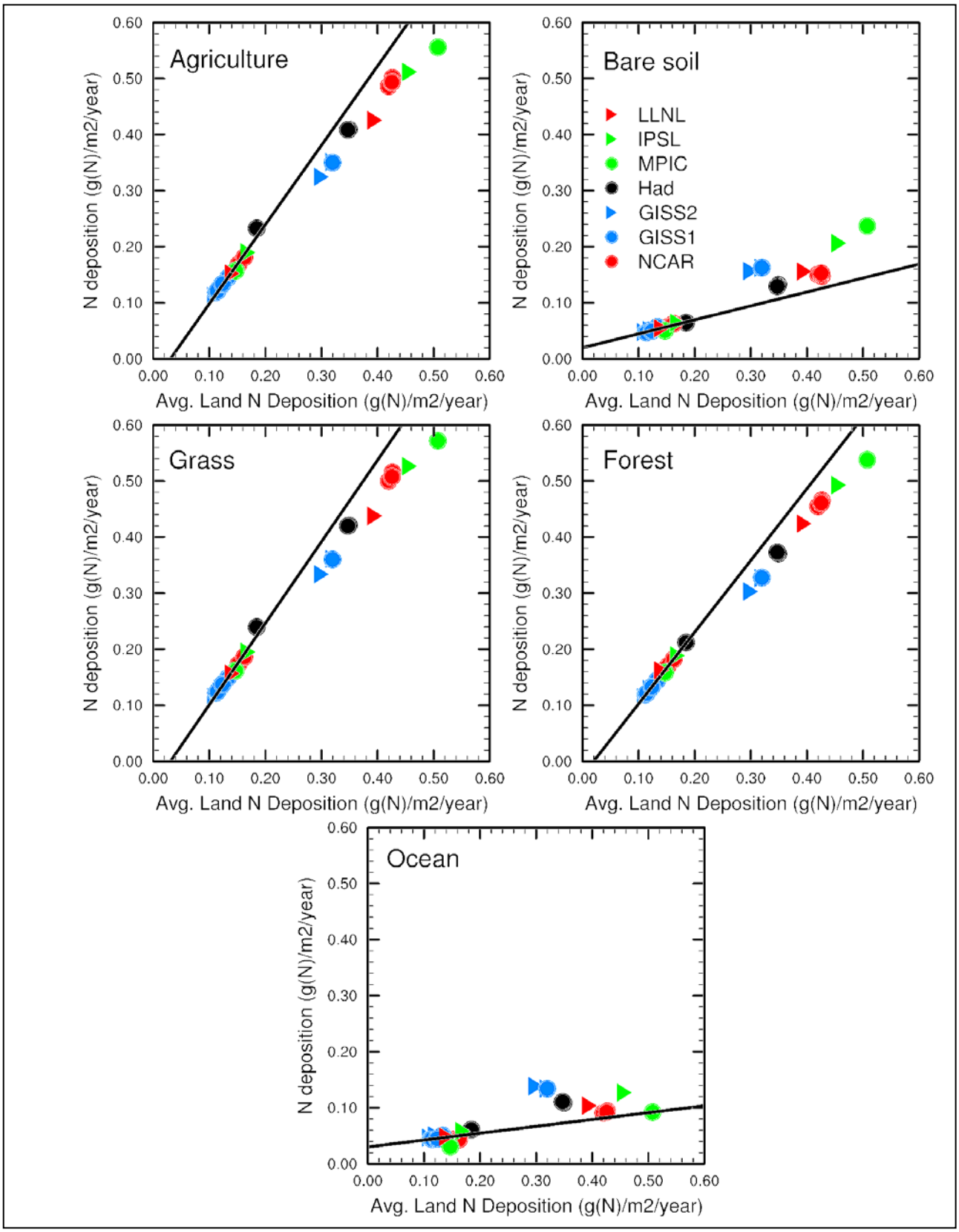
Agriculture
Bare soil
Grass
Forest
Ocean
LLNL
IPSL
MPIC
Had
GISS2
GISS1
NCAR
N deposition (g(N)/m2/year)
Avg. Land N Deposition (g(N)/m2/year)
0.00
0.10
0.20
0.30
0.40
0.50
0.60

Figure 6

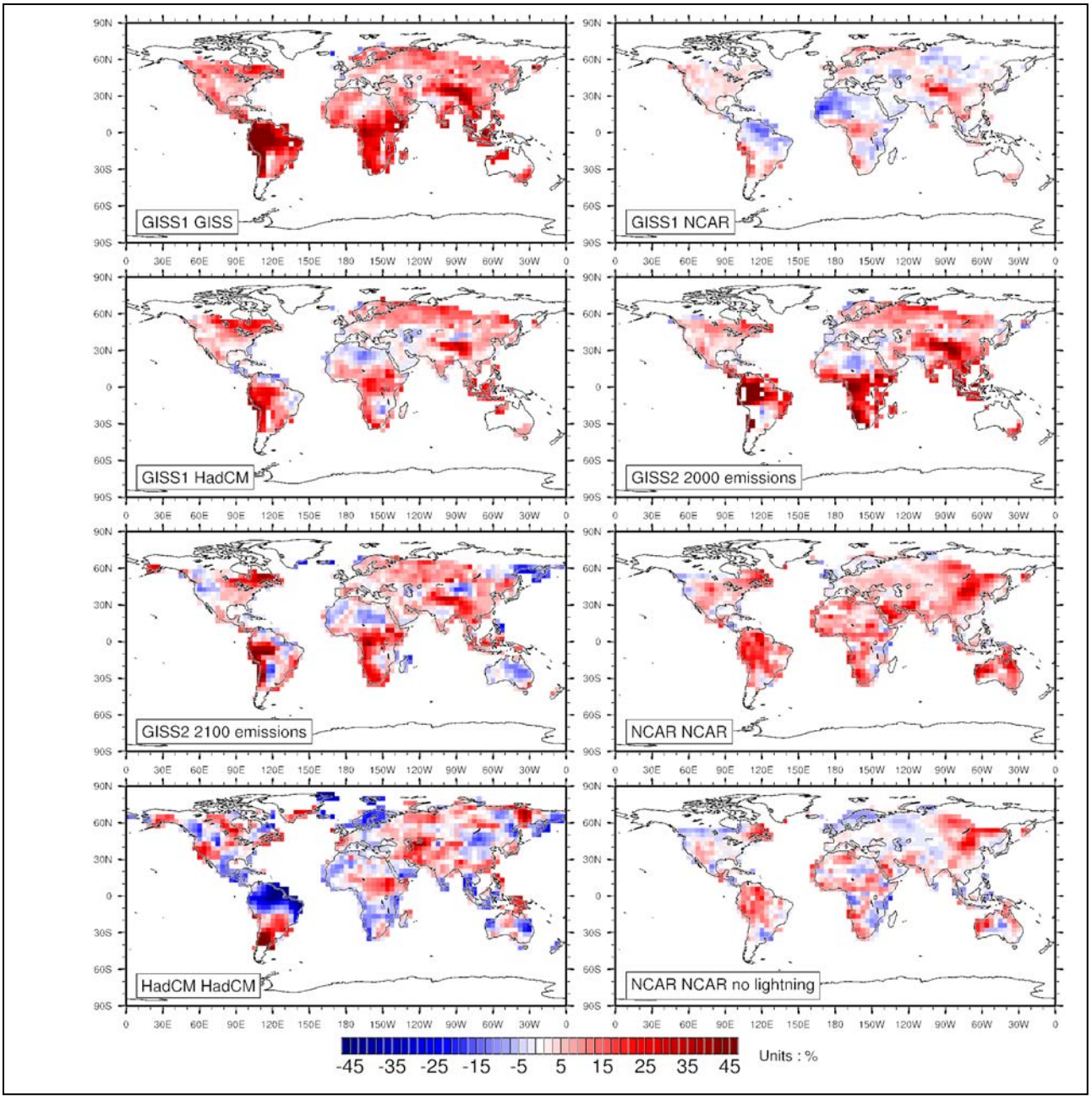
GISS1 GISS
GISS1 NCAR
GISS1 HadCM
GISS2 2000 emissions
GISS2 2100 emissions
NCAR NCAR
HadCM HadCM
NCAR NCAR no lightning
-45 -35 -25 -15 -5 5 15 25 35 45
Units : %

Figure 7

View publication stats